

Analysis of the first high-gain harmonic-generation free-electron laser at saturation

M. Babzien, I. Ben-Zvi, L.F. DiMauro, A. Doyuran, W. Graves, E. Johnson, S. Krinsky, R. Malone, I. Pogorelsky, G. Rakowsky, T. Shaftan, J. Skaritka, X.J. Wang, M. Woodle, V. Yakimenko, and L.H. Yu
Brookhaven National Laboratory, Upton, New York 11973

S.G. Biedron, J. Jagger, V. Sajaev, and I. Vasserman
Advanced Photon Source, Argonne National Laboratory, Argonne, Illinois 60439

We report results from characterization of the output of a high-gain harmonic-generation (HGFG) free-electron laser (FEL). A CO₂ seed laser at a wavelength of 10.6 μm is amplified and frequency-doubled in the FEL to produce 5.3-μm output. The wavelength spectrum, pulse duration, and correlation length of the output verify that the light is longitudinally coherent. Comparisons of the measured electron energy distribution and the nonlinear harmonics of the 5.3-μm radiation with values obtained from numerical models are consistent with saturated HGFG FEL operation. In addition, a brief discussion of the extension of this technique to ever-shorter wavelengths as well as wavelength tailoring for specific experiments will be discussed.

PACS Codes: 41.60.Cr

There is great interest in the production of short-pulse radiation at deep UV and X-ray wavelengths and intensities exceeding those achieved with conventional lasers [1,2]. A natural candidate to produce such radiation is the free-electron laser (FEL). One approach that has been the subject of widespread theoretical and experimental investigation [3-12] is called self-amplified spontaneous emission (SASE). In the SASE process the spontaneous radiation emitted by quivering electrons near the beginning of a long undulator magnet is subsequently amplified as it copropagates with the electron beam through the magnet structure. A SASE FEL can produce short wavelength light with high peak power and excellent spatial mode. However, the light has poor temporal coherence (coherence time much shorter than the pulse duration) and chaotic shot-to-shot variations since the process is initiated through shot noise.

Recently, another single-pass FEL approach using the high-gain harmonic-generation (HGFG) scheme, which is capable of producing longitudinally coherent pulses, was demonstrated [13-16]. In an HGFG FEL the light output is derived from a coherent subharmonic seed pulse. Consequently, the optical properties of the HGFG FEL are a map of the characteristics of the high-quality seed laser. This has the benefit of providing light with a high degree of stability and control of the central wavelength, bandwidth, energy, and pulse duration that is absent from a SASE source. Furthermore, the HGFG source can produce light pulses with durations much shorter than the electron bunch length by synchronizing an ultrashort laser pulse to the electron beam. In this paper we show through a series of measurements that the output of an HGFG FEL is saturated and longitudinally coherent. The experiments give good agreement with values obtained from theoretical simulations [17].

The experiments [15,16] were performed at the Accelerator Test Facility (ATF) at Brookhaven National Laboratory in collaboration with the Advanced Photon Source at Argonne National Laboratory. The principle of the HGFG FEL was influenced by earlier work in the field [18-22], but differs from previous approaches in that the harmonic radiation is exponentially amplified. The experimental layout shown in Fig. 1 illustrates the interaction of a 200-ps-long, 10.6- μm seed pulse from a CO_2 laser with the 6-ps-long electron beam. The seed light has a Rayleigh range of 0.8 m and a half-intensity beam diameter of 1.7 mm. The amplification process in the CO_2 laser limits the bandwidth of the seed pulse and results in a pulse duration much longer than the electron bunch length. Therefore, the short slice of the laser seed pulse acting on the electron bunch possesses a very high degree of temporal coherence. The resonant interaction of the seed laser and electron bunch in the first (modulator) undulator results in an energy modulation that is converted to a spatial bunching when the electron beam traverses the dispersion section (a three-dipole chicane). In the second (radiator) undulator, tuned to be resonant at 5.3 μm , the microbunched electron beam first emits coherent radiation and then amplifies it exponentially until saturation is achieved. First lasing of an HGFG FEL was reported in refs. [15, 16]. The HGFG pulse energy was measured to be $\sim 10^7$ times larger than the spontaneous radiation and 10^6 times larger than the SASE signal, which, in the case of the HGFG experiment, is a source of background noise. The single-shot spectral distribution of the HGFG output near 5.3 μm was recorded by placing a thermal imaging camera at the exit plane of a spectrometer. The full-width half-maximum (FWHM) bandwidth of the HGFG output was found to be 15 nm [16], much narrower than the

SASE bandwidth. In this paper, we extend the earlier work by using a second-harmonic autocorrelator to measure the intensity pulse duration and an interferometer to measure the coherence length. The agreement of these two measurements indicates that the excellent longitudinal coherence of the seed laser is mapped to the HGHG output.

Numerical simulation [17] employing parameters similar to the current experiment was carried out using a modified version of the Three-Dimensional Axis-symmetric (TDA) code [14]. In this model, the radiation process is simulated using the Maxwell equations coupled to the classical equations describing the electron motion. A Monte Carlo method provides a random distribution of the initial conditions. Our model assumes that slippage effects are negligible since the electron bunch length (6 ps) is longer than the slippage distance (1 ps).

In the HGHG process, energy modulation of the electron beam is generated in two ways: through the initial interaction of the seed laser with the electron beam in the modulator and through the HGHG FEL interaction in the radiator. The energy modulation produced in the radiator dominates. The amount of modulation is measured using an electron energy spectrometer after the radiator section. Due to the dispersion of the bending magnet downstream of the HGHG radiator undulator, the electrons with different energies will follow different trajectories. By adjusting the quadrupole strength to minimize the betatron motion in the horizontal direction, one can correlate the electron's position with energy and thus measure the energy distribution.

The electron beam energy distributions at the spectrometer with the CO₂ laser on (solid line) and with the CO₂ laser off (dashed line) are shown in Fig. 2. The effect of the CO₂ laser on the electron beam is dramatic, producing an energy modulation of $\Delta\gamma/\gamma=2.5\%$. Using conditions similar to the experiment, the simulation [17] shows that the double peak distribution in Fig. 2 is a signature of saturation in the radiator undulator. In addition, with the CO₂ laser on, the center of mass of the beam in Fig. 2 shifts to the right by $\Delta\gamma/\gamma=0.167\%$. For a 120-amp, 40-MeV electron beam, this shift corresponds to 50 μJ of total energy loss, which is our typical measured HGHG output energy, consistent with the conservation of energy.

Further evidence of saturation is obtained by measuring the pulse energy of the second-harmonic (2.65 μm) and the third-harmonic (1.77 μm) components relative to the energy of the radiator fundamental (5.3 μm). The fundamental and harmonic light were measured using an InSb detector with a calibrated spectral response. Comparable detector signal levels were produced using appropriate bandpass and neutral density filters. In Fig. 3, we plot the output energy (μJ) for the fundamental and first two harmonics versus electron beam energy modulation (%). As evident in the data, simulations [23-26] predict that the onset of an exponential increase in the harmonic energy at 2.65 μm and 1.77 μm as the electron energy modulation approaches 2.5% is strong evidence of saturation. In Table 1, the numerical results [26] and the experimental measurements of the ratio of the harmonic-to-fundamental energies are presented for a 2.5% electron beam energy modulation. Good agreement is found between experiment and theory.

Table 1: The theoretical and experimentally measured harmonic-to-fundamental ratios.

Wavelength	Simulation	Experiment
2.65 μm	6×10^{-4}	2×10^{-4}
1.77 μm	1×10^{-2}	0.8×10^{-2}

An important attribute of the HGHG approach in contrast to SASE is the excellent longitudinal coherence of the output. A series of experiments was performed characterizing the temporal output properties of the HGHG FEL. The pulse duration of the 5.3- μm HGHG pulse was studied using a standard scanning, background-free, second-harmonic optical autocorrelator configuration. The small group velocity mismatch of the 1-mm-thick AgGaSe₂ doubling crystal and geometric beam overlap in the crystal resulted in an instrumental resolution of better than 0.5 ps. The main sources of error in the measurement are imposed by the low-duty cycle of the CO₂ laser (0.05 Hz) and instabilities in the electron beam. In order to reduce scatter, each data point is a single-shot measurement of the second harmonic signal normalized to the square of the fundamental energy. The normalized signal versus delay time (relative length difference between the two arms of the Michelson) is shown in Fig. 4. Assuming a Gaussian pulse shape, the duration is found to be $8.4/\sqrt{2} = 5.9 \pm 0.7$ ps. A transform-limited Gaussian pulse [27] will produce a FWHM time-bandwidth ($\Delta f \Delta t$) product equal to $2 \ln 2 / \pi$. In this experiment, the measured pulse duration and bandwidth of 15 nm yields a $\Delta f \Delta t$ product that is a factor of two larger than a Gaussian. More generally though, the value of the $\Delta f \Delta t$ product depends on the exact shape of the pulse, e.g., a flat-top pulse gives a $\Delta f \Delta t \approx 0.9$. Clearly the limitations imposed by the scatter in the current experiment prohibit such a determination. However, short wavelength HGHG experiments planned at Brookhaven should result in a more complete optical characterization. Using the value of 5.9 ps for the HGHG output pulse and the measured energy of 100 μJ gives an output power of 17 MW, which is within a factor of two of the theoretical prediction [17] of 35 MW. Consistent with the earlier discussion, the simulation [17] also predicts deep saturation at this output power.

In another experiment, a modified Michelson interferometer was used to investigate the temporal coherence of the 5.3- μm HGHG output. The retroreflecting mirror in one arm of the interferometer was tilted and then translated while the fringe visibility of the interference pattern was recorded on a thermal imaging camera. In order to collect more light, we added a cylindrical mirror to produce a line-type image on the thermal camera. In the interferogram, the visibility [27] is defined as $\frac{I_{\max} - I_{\min}}{I_{\max} + I_{\min}}$ where

I_{\max} and I_{\min} are the maximum and minimum average intensity, respectively, in the center of the fringe pattern. The variation of fringe visibility as a function of delay,

plotted in Fig. 5, is a measure of the coherence length of the pulse. The FWHM of the Gaussian fit in Fig. 5 yields a coherence time of 5.4 ± 0.5 ps.

The determination of the exact degree of longitudinal coherence is problematic since the correlation function [27] is dependent on the temporal profile, e.g., Gaussian, flat-top, etc. Just like the autocorrelation measurement, fluctuations in the HGHG source predominantly introduced by instabilities in the electron beam and CO₂ laser severely limit the accuracy of the measurement and our ability to discriminate line profiles. However, the agreement in the measured pulse duration and coherence time reveals that the HGHG pulse is temporally coherent across its intensity profile. This is further corroborated by the close agreement in the time-bandwidth product. Although our measurement is unable to determine the exact nature of the output pulse, it is clear that it has a high degree of longitudinal coherence.

In conclusion, we measured the characteristics of a saturated HGHG FEL. The results demonstrate the utility of HGHG for producing intense coherent light pulses. Saturated FEL performance is confirmed by the extent of energy modulation introduced into the electron beam and the output energy of the harmonics and FEL fundamental light. Second-harmonic autocorrelation, interferometry and spectral measurements confirm that an HGHG FEL output is longitudinally coherent. The measurements are found to be consistent with theoretical simulations, which can provide an important roadmap toward short-wavelength operation. Higher-order even and odd harmonics of the seed radiation may be amplified to high power by adjusting the relative resonance conditions between the modulator and radiator. Furthermore, simulations show that the cascading of HGHG stages [28-32] can result in comparable hard X-ray production as a SASE FEL under similar operational parameters but with fully coherent output. A step towards this regime is currently being taken at Brookhaven with the extension of HGHG into the VUV.

We thank all ATF personnel for their great help in making this experiment a success. This work was supported by U.S. Department of Energy, Office of Basic Energy Sciences, under Contracts Nos. DE-AC02-98CH10886 and W-31-109-ENG-38 and by Office of Naval Research Grant No. N00014-97-1-0845.

References

- [1] S. Leone, "Report of the BESAC Panel on Novel Coherent Light Sources" (U.S. Department of Energy, Washington D.C., 1999).
- [2] "Linac Coherent Light Source (LCLS) Design Study Report," The LCLS Design Study Group, Stanford Linear Accelerator Center (SLAC) Report No. SLAC-R-521, 1998.
- [3] Y.S. Debenev, A.M. Kondratenko and E.L. Saldin, Nucl. Instrum. Methods A 193, 415 (1982).
- [4] R. Bonifacio, C. Pellegrini, and L. Narducci, Opt. Commun. 50, 373 (1984).
- [5] J.M. Wang and L.H. Yu, Nucl. Instrum. Methods A 250, 484 (1986).
- [6] K. J. Kim, Nucl. Instrum. Methods A 250, 396 (1986).
- [7] K.J. Kim, Phys. Rev. Lett. 57, 1871 (1986).
- [8] S. Krinsky and L.H. Yu, Phys. Rev. A 35, 3406 (1987).
- [9] L.H. Yu, S. Krinsky, and R.L. Gluckstern, Phys. Rev. Lett. 64, 3011 (1990).
- [10] SASE gain of 10^5 at 12 μm was reported in M. J. Hogan et al., Phys. Rev. Lett. 22, 4867 (1998).
- [11] SASE gain at 530 nm was observed at the LEUTL facility at APS/ANL, S.V. Milton et al., Phys. Rev. Lett. 85, 988 (2000).
- [12] SASE gain at 110 nm was observed at TTF/DESY, J. Andruszhow, Phys. Rev. Lett. 85, 3825 (2000).
- [13] I. Ben-Zvi et al., Nucl. Instrum. Methods A 304, 151 (1991).
- [14] L.H. Yu, Phys. Rev A 44, 5178 (1991).
- [15] L.-H. Yu et al., Nucl. Instrum. Methods A 445, 301 (2000).
- [16] L.-H. Yu et al., Science 289, 932 (2000).
- [17] L.-H. Yu, Proc. 1999 Particle Accelerator Conference, New York, March 27-April 2, 1999, p 2474.
- [18] I. Boscolo and V. Stagno, Nucl. Instrum. Methods A 188, 483 (1982).

- [19] I. Schnitzer and A. Gover, Nucl. Instrum. Methods A 237, 124 (1985).
- [20] R. Bonifacio et al., Nucl. Instrum. Methods A 296, 787 (1990).
- [21] R. Prazeres et al., Nucl. Instrum. Methods A 304, 72 (1991).
- [22] D.A. Jaroszynski et al., Nucl. Instrum. Methods A 375, 456 (1996).
- [23] R. Bonifacio, L. De Salvo and P. Pierini, Nucl. Instrum. Methods A 293, 627 (1990).
- [24] H.P. Freund, S.G. Biedron, S.V. Milton, IEEE J. Quantum Electron. 36, 275 (2000).
- [25] Z. Huang and K.J. Kim, Proc. 22nd International FEL Conference, Duke University, Durham, NC, August 13-18, 2000.
- [26] S.G. Biedron et al., Proc. 22nd International FEL Conference, Duke University, Durham, NC, August 13-18, 2000.
- [27] L. Mandel and E. Wolf, *Optical Coherence and Quantum Optics* (Cambridge University Press, 1995) p. 166.
- [28] I. Ben-Zvi et al., Nucl. Instrum. Methods A 393, II-10 (1997).
- [29] L. H. Yu and I. Ben-Zvi, Nucl. Instrum. Methods A 393, 96 (1997).
- [30] L.H. Yu and J.H. Wu, "Harmonic generation of hard X-rays," Proc. of the ICFA Advanced Beam Dynamics Workshop on Future Light Sources, C.E. Eyberger, ed., Argonne National Laboratory, Argonne, IL (1999), (available at URL: <http://www.aps.anl.gov/conferences/FLSworkshop/proceedings/papers/wg1-01.pdf>).
- [31] J.H. Wu and L.H. Yu, Proc. 22nd International FEL Conference, Duke University, Durham, NC, August 13-18, 2000.
- [32] S.G. Biedron, S.V. Milton and H.P. Freund, Proc. 22nd International FEL Conference, Duke University, Durham, NC, August 13-18, 2000.

Figure Captions

Figure 1: HGHG experimental schematic and typical parameters. The accelerator produces 6-ps, 40-MeV electron pulses with a peak current of 120 A, emittance (ϵ) and energy spread ($d\gamma/\gamma$). Listed are the length (L), period (λ), and magnetic field (B) for the modulator and radiator. The dispersive section is 0.3 m long with a dispersion of $d\Psi/d\gamma$.

Figure 2: The energy distribution of the electron beam after the electron spectrometer with (solid line) and without (dashed line) the CO₂ laser beam. The energy modulation is defined as the FWHM of the beam distribution. On the horizontal axis, positive values correspond to electron energy loss.

Figure 3: Harmonic energy (μJ) versus electron beam energy modulation (%). The (\bullet)s are the data for the 5.3- μm fundamental and the solid line is a linear fit. The energies for the second (+) and third (o) harmonics are multiplied by 10^3 and 10^2 , respectively. The second (dashed line) and third (dotted line) harmonic energy growth are fit by an exponential. Fits are constrained to a zero crossing.

Figure 4: The second-harmonic autocorrelation trace of the 5.3- μm HGHG output. The FWHM pulse width is 5.9 ± 0.7 ps as determined by a Gaussian fit.

Figure 5: The coherence length of the HGHG radiation pulse measured by plotting the fringe visibility as a function of delay. The solid curve is a Gaussian fit with an FWHM coherence time of 5.4 ± 0.5 ps.

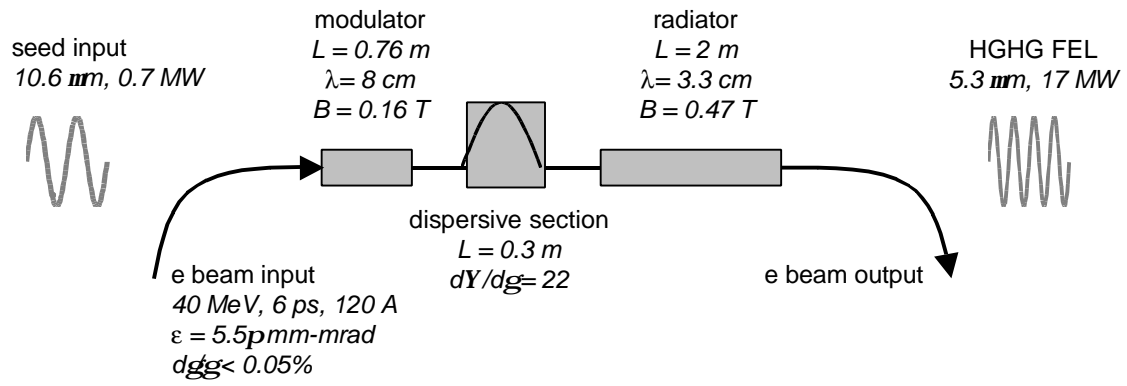


Figure 1 (Babzien et al.)

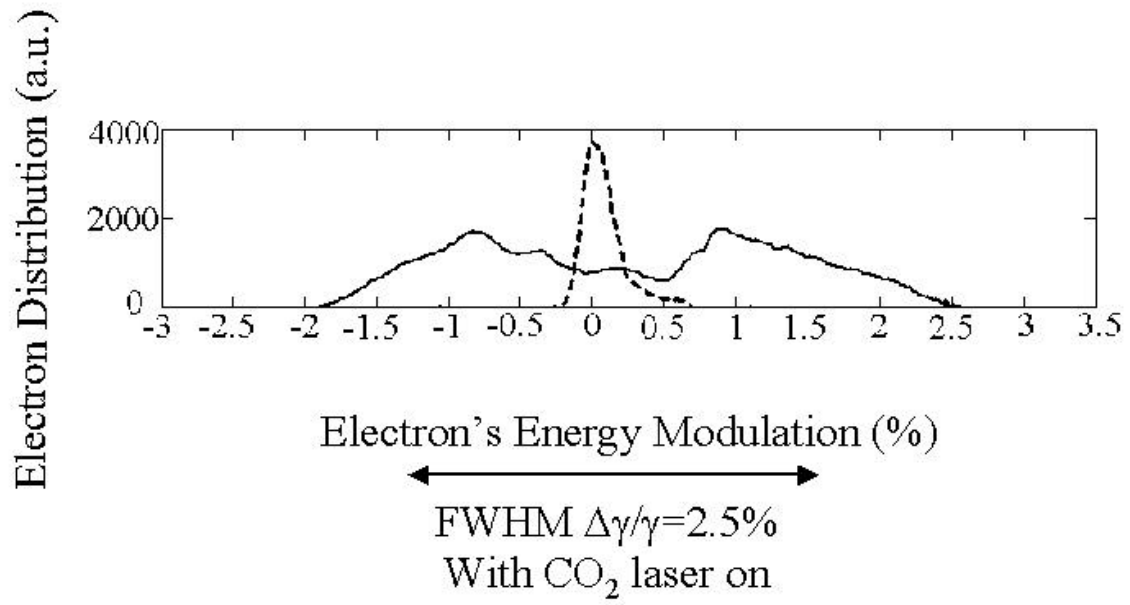


Figure 2 (Babzien et al.)

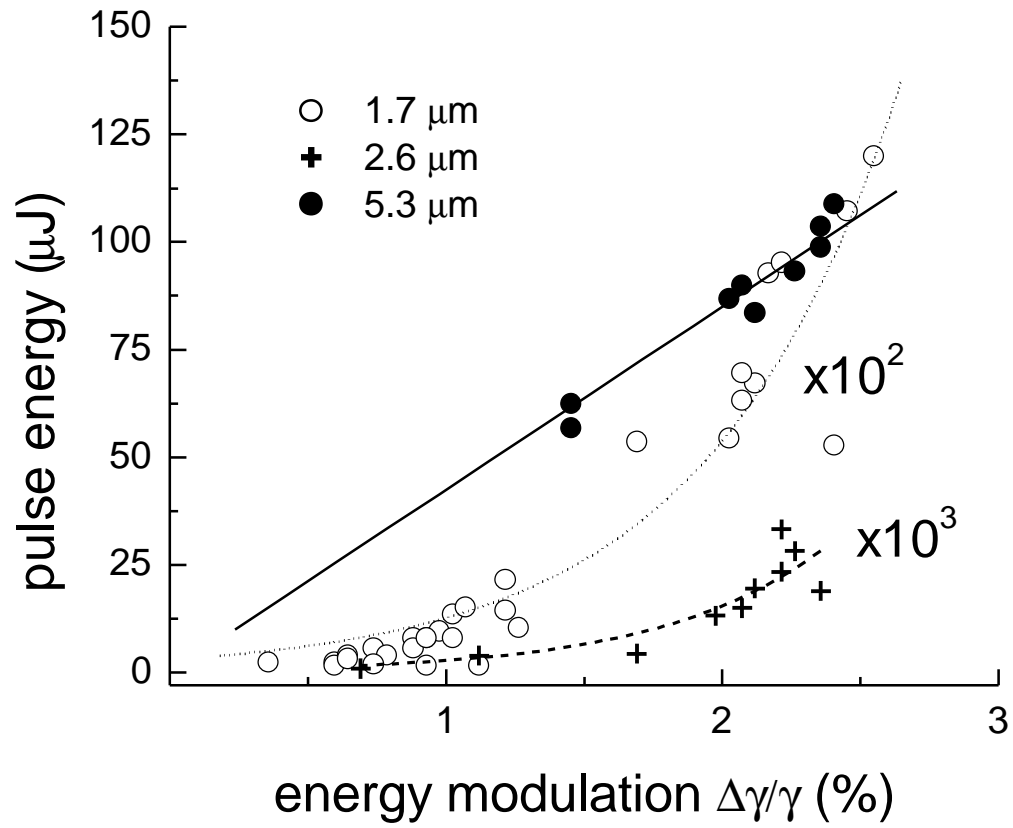


Figure 3 (Babzien et al.)

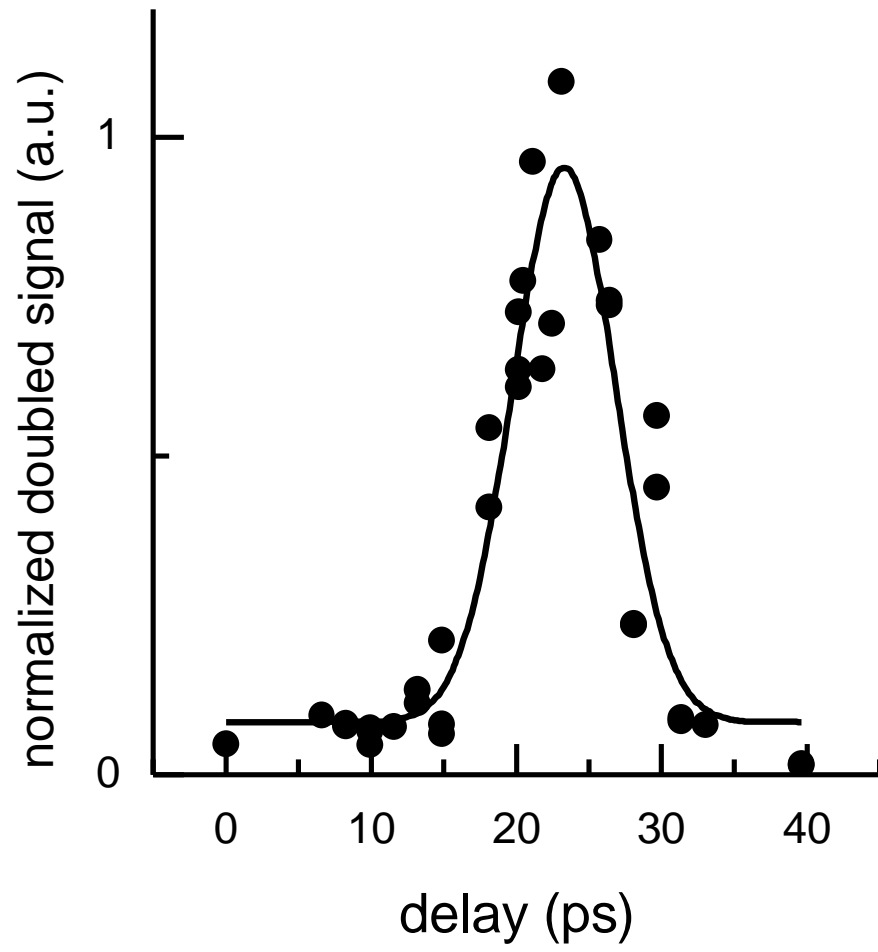


Figure 4 (Babzien et al.)

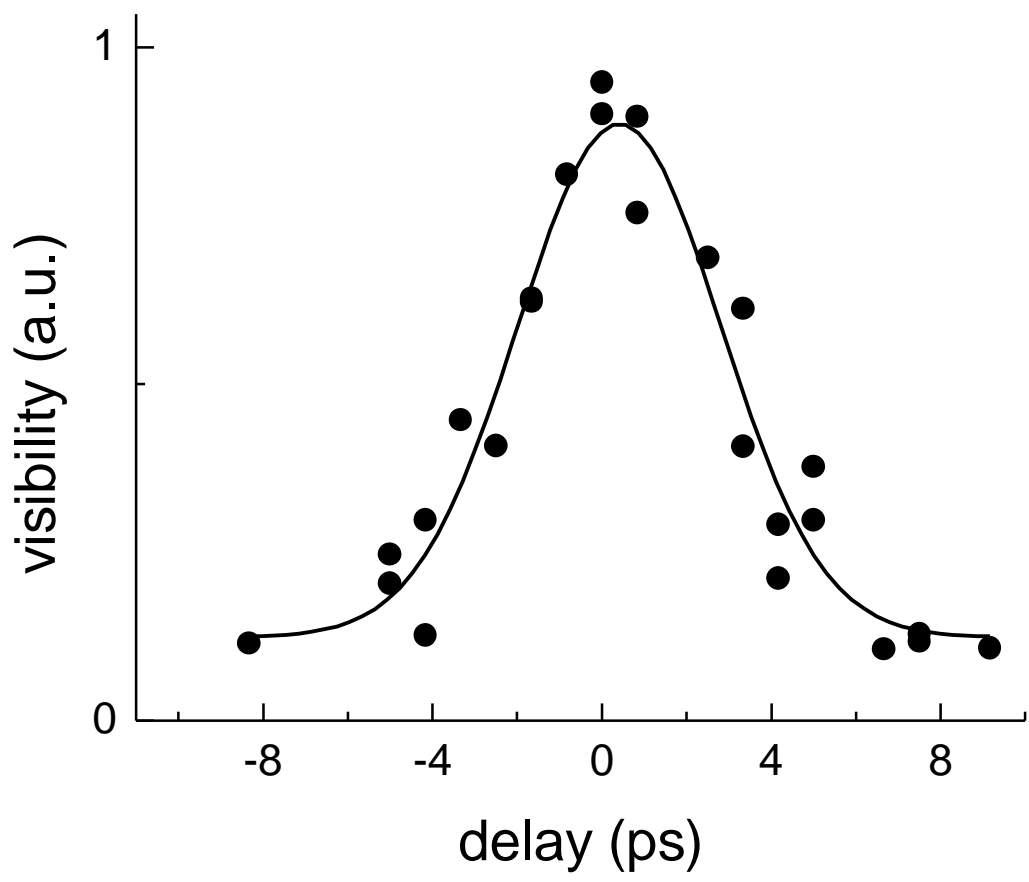


Figure 5 (Babzien et al.)